PERGAMON

International Journal of Solids and Structures 37 (2000) 4557–4575

INTERNATIONAL JOURNAL OF SOLIDS and STRUCTURES

www.elsevier.com/locate/ijsolstr

An elliptic inclusion with imperfect interface in anti-plane shear

H. Shen, P. Schiavone*, C.Q. Ru, A. Mioduchowski

Department of Mechanical Engineering, University of Alberta, Edmonton, Alberta, Canada T6G 2G8

Received 25 November 1998; in revised form 8 March 1999

Abstract

A semi-analytic solution is developed for the problem associated with an elliptic inclusion embedded within an infinite matrix in anti-plane shear. The bonding at the inclusion-matrix interface is assumed to be homogeneously imperfect. The interface is modeled as a spring (interphase) layer with vanishing thickness. The behaviour of this interphase layer is based on the assumption that tractions are continuous but displacements are discontinuous across the interface. Complex variable techniques are used to obtain infinite series representations of the stresses induced within the inclusion. The results obtained demonstrate how the (non-uniform) stress field and the average stresses inside the inclusion vary with the aspect ratio of the inclusion and the parameter describing the imperfect interface. In addition, it is shown that, in some cases (depending on the aspect ratio of the ellipse), it is possible to identify specific values of the interface parameter which correspond to maximum peak stress along the interface.

Keywords: Elliptic inclusion; Imperfect interface; ANM-plane shear

1. Introduction

Problems involving elastic inclusions with imperfect bonding at the inclusion-matrix interface (imperfect interface) have received a considerable amount of attention in the literature (see, Ru and Schiavone (1997) for a recent survey and bibliography). Interest in these problems is motivated by the study of interface damage in composites (for example, debonding, sliding and/or cracking across an interface) and its subsequent effect on the effective properties of composites.

One of the more widely used models of an imperfect interface (see, for example, Aboudi, 1987;

* Corresponding author. Fax: +1-780-492-2200.
E-mail address: P.Schiavone@ualberta.ca (P. Schiavone).

0020-7683/00/$ - see front matter
PII: S0020-7683(99)00174-2

Achenbach and Zhu, 1989; Hashin, 1990, 1991a,b, 1992; Gao, 1995; Ru and Schiavone, 1997) is based on the assumption that tractions are continuous but displacements are discontinuous across the interface. More precisely, jumps in the displacement components are assumed to be proportional, in terms of 'spring-factor-type' interface parameters, to their respective interface traction components. When these interface parameters are assumed to be uniform along the entire length of the material interface, the interface model is said to represent a *homogeneously imperfect interface*. Using this model, Hashin (1991b) examined the case of a spherical inclusion imperfectly bonded to a three-dimensional matrix. In contrast to the case of perfect bonding (see, for example, Eshelby, 1957), Hashin found that, under a remote uniform stress field, the state of stress inside the inclusion is no longer uniform. The analogous result in plane elasticity has been established by Gao, 1995 for a circular inclusion (see also Qu, 1993) for similar results concerning an elliptic inclusion with a 'slightly weakened interface'). To our knowledge, despite its importance to composite mechanics and the study of elastic inclusions with imperfect interfaces, the solution of the problem of an *elliptic* inclusion with *homogeneously imperfect interface* has not been recorded in the literature.

In the present work, we consider the problem associated with an elliptic elastic inclusion embedded within an infinite matrix in anti-plane shear, when the interface is homogeneously imperfect. Using complex variable techniques we obtain infinite series representations of the corresponding stresses which, when evaluated numerically, demonstrate how the (non-uniform) stress field and the average stress within the inclusion vary with the parameter describing the imperfect interface. In addition, we show that, in some cases (depending on the aspect ratio of the inclusion), interfacial stresses are found to be non-monotonic functions of the interface parameter. In these cases, it is possible to identify specific values of the interface parameter which correspond to maximum peak stress along the interface.

2. Problem formulation

Consider a domain in R^2, infinite in extent, containing a single internal elastic inclusion, with elastic properties different from those of the surrounding matrix. The linearly elastic materials occupying the matrix and inclusion are assumed to be homogeneous and isotropic with associated shear moduli μ^1 and μ^2, respectively. At infinity, the prescribed deformation is that of a simple shear. We represent the matrix by the domain S_1 and assume the inclusion occupies an elliptic region S_2. The ellipse Γ will denote the inclusion-matrix interface. In what follows, the subscripts 1 and 2 will refer to the regions S_1 and S_2, respectively, (x, y) is a generic point in R^2 and $w(x, y)$ will denote the elastic (anti-plane) deformation at the point (x, y).

We assume that the interface is homogeneously imperfect as described in Section 1. The interface condition is therefore given by (see Ru and Schiavone, 1997)

$$h\big[w_1 - (w_2 + \omega^*)\big] = \mu_1 \frac{\partial w_1}{\partial n} = \mu_2 \frac{\partial w_2}{\partial n}, \quad \text{on } \Gamma, \tag{1}$$

where h = constant is the imperfect interface parameter, n is the outward unit normal to Γ and $\omega^*(x,y)$ represents the additional displacement induced within the inclusion by a uniform eigenstrain specified below. We note that as h approaches infinity in Eq. (1), we must have $w_1 = w_2 + \omega^*(x, y)$ so that, in this case, Eq. (1) describes a perfectly bonded interface (see, for example, Ru and Schiavone, 1996). Similarly, if $h = 0$, Eq. (1) reduces to the case of a traction-free interface, which characterizes the complete debonding of the inclusion from the matrix. Consequently, the following boundary value problem describes anti-plane shear deformations of an elliptic inclusion with the imperfect interface of the form (1) (see Ru and Schiavone, 1997):

$$\nabla^2 w_1 = 0, \quad in\ S_1, \qquad \nabla^2 w_2 = 0, \quad in\ S_2$$

$$h[w_1 - w_2] = \mu_2 \frac{\partial w_2}{\partial n} + h\omega^*, \qquad \mu_1 \frac{\partial w_1}{\partial n} = \mu_2 \frac{\partial w_2}{\partial n} \quad \text{on } \Gamma$$

$$w_1(x,y) \cong c_1 x - c_2 y + 0(1), \qquad x^2 + y^2 \to \infty \tag{2}$$

Here, c_α, $\alpha = 1, 2$ are given constants (remote stress parameters).

We denote the complex potentials corresponding to $w_\alpha(x, y)$, $\alpha = 1, 2$, by $\Phi_1(z)$ and $\Phi_2(z)$, respectively. Since $\Phi_1(z)$ and $\Phi_2(z)$ are analytic within S_1 and S_2, respectively, we can write,

$$2w_k = \Phi_k(z) + \overline{\Phi_k(z)}$$

$$\sigma_{xz} - i\sigma_{yz} = \mu_k \Phi_k'(z) \quad z \in S_k\ (k = 1, 2) \tag{3}$$

where σ_{xz} and σ_{yz} represent the corresponding stress components in anti-plane shear. Noting that

$$2\frac{\partial w_2}{\partial n} = \Phi_2'(z)\, \mathrm{e}^{in(z)} + \overline{\Phi_2'(z)}\, \mathrm{e}^{-in(z)}, \quad z \in \Gamma,$$

where, $\mathrm{e}^{in(z)}$ represents (in complex form) the outward unit normal to Γ at z. The boundary value problem (2) can now be re-written in complex form as:

$$\Phi_1(z) = \delta\Phi_2(z) + (1-\delta)\overline{\Phi_2(z)} + \alpha\left[\Phi_2'(z)\, \mathrm{e}^{in(z)} + \overline{\Phi_2'(z)}\, \mathrm{e}^{-in(z)}\right] + \omega^*(z), \quad z \in \Gamma$$

$$\Phi_1(z) \cong Az + 0(1), \quad |z| \to \infty. \tag{4}$$

Here

$$A \equiv c_1 + ic_2, \alpha = \frac{\mu_2}{2h} \geq 0, \delta \equiv \frac{\mu_1 + \mu_2}{2\mu_1} > \frac{1}{2}, \omega^* = \omega z + \overline{\omega z} \tag{5}$$

and ω is a known complex constant determined by the uniform eigenstrain given in the inclusion.

3. Conformal mapping

Let Γ be an ellipse with centre at the origin of the complex z-plane, semi-major and semi-minor axes a and b, respectively and foci at $x = \pm 2R$, $R > 0$. Consider the following conformal mapping from the complex z-plane to the complex ξ-plane (Muskhelishvili, 1963):

$$z = m(\xi) = R\left(\xi + \frac{1}{\xi}\right), R = \frac{\sqrt{a^2 - b^2}}{2} > 0, \xi = \zeta + i\eta = r\, \mathrm{e}^{i\theta} \tag{6}$$

As illustrated in Fig. 1, we imagine the enclosed region S_2 to be cut along the segment $D_1 = \{(x, 0): -2R \leq x \leq 2R\}$ connecting the foci of the ellipse. This cut may be thought of as an ellipse, which is confocal with Γ but whose minor axis is zero. Hence, the cut region in S_2 may be thought of as the limiting case of a region between two confocal ellipses.

Using Eq. (6), we map the ellipse $x = R(R^* + \frac{1}{R^*})\cos\theta$, $y = R(R^* - \frac{1}{R^*})\sin\theta$ and its exterior region in

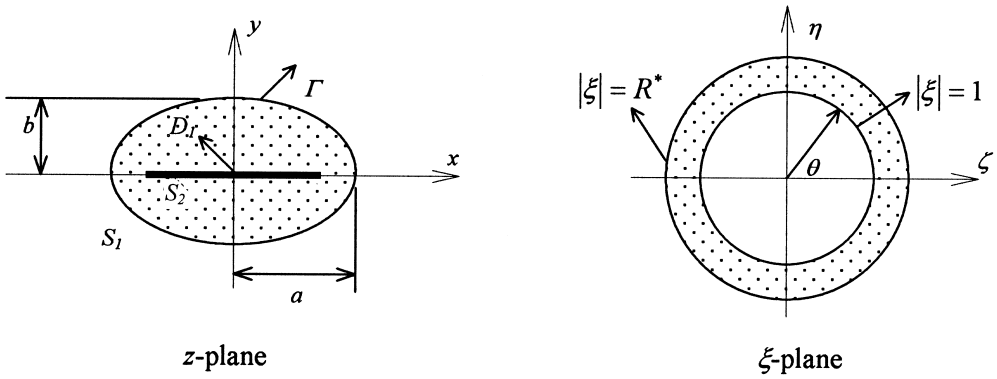

Fig. 1. The conformal mapping from z-plane to ζ-plane.

the complex z-plane, onto and outside, respectively, the circle of radius R^* in the complex ξ-plane. Here

$$R^* = \frac{a + \sqrt{a^2 - 4R^2}}{2R} = \sqrt{\frac{a+b}{a-b}} > 1 \tag{7}$$

Since, $\Phi_2(z)$ is analytic in S_2, it follows that

$$\Phi_2(z) = \Phi_2(\overline{z}), \quad z \in D_1 \tag{8}$$

4. General solution

For convenience, we write

$$\Phi_\alpha(z) = \Phi_\alpha(m(\xi)) = \Phi_\alpha(\xi), \quad \alpha = 1,2,$$

so that, in the ξ-plane, condition (8) becomes

$$\Phi_2(\xi) = \Phi_2\left(\overline{\xi}\right), \quad \forall \xi : |\xi| = 1$$

Using (6), writing $\xi = re^{i\theta}$ and noting that (England, 1971)

$$e^{i2n(z)} = \frac{\xi^2}{r^2}\frac{m'(\xi)}{\overline{m'(\xi)}}, \; e^{in(z)} = \frac{\xi}{r}\frac{m'(xi)}{|m'(\xi)|}, \; e^{-in(z)} = \frac{\overline{\xi}}{r}\frac{\overline{m'(\xi)}}{|m'(\xi)|},$$

the problem (4) reduces to finding analytic functions $\Phi_\alpha(\xi)$, $\alpha = 1, 2$ in the regions $\xi > R^*$ and $1 < \xi < R^*$, respectively, such that

$$\Phi_1(\xi) = \delta\Phi_2(\xi) + (1-\delta)\overline{\Phi_2(\xi)} + \beta\left[\xi\Phi_2'(\xi) + \overline{\xi}\Phi_2'(\xi)\right] + \omega m(\xi) + \overline{\omega m(\xi)}, |\xi| = R^*, \tag{9}$$

$$\Phi_2(\xi) = \Phi_2\left(\overline{\xi}\right), \quad |\xi| = 1, \tag{10}$$

$$\Phi_1(\xi) \cong AR\xi + 0(1), \quad |\xi| \to \infty. \tag{11}$$

Here,

$$\beta(\theta) = \frac{\alpha}{R^*|m'(\xi)|} = \frac{\alpha}{b\sqrt{1 + b^* \sin^2\theta}}, \quad b^* = \frac{a^2 - b^2}{b^2} > 0 \tag{12}$$

Since $\Phi_1(\xi)$ is analytic in $|\xi| > R^*$, using Eq. (11), it can be represented there by the following Laurent series

$$\Phi_1(\xi) = AR\xi + \sum_{n=0}^{\infty} d_n \xi^{-n} \tag{13}$$

where d_n are unknown coefficients to be determined. Similarly, $\Phi_2(\xi)$ is analytic in the ring $1 < |\xi| < R^*$, and hence has Laurent series representation

$$\Phi_2(\xi) = \sum_{n=-\infty}^{\infty} b_n \xi^n \tag{14}$$

where, again, b_n are unknown constants to be determined.

From Eq. (10), letting $\xi = r\,\mathrm{e}^{i\theta}$ we obtain (see, for example, Muskhelishvili, 1963)

$$b_n = b_{-n}, \quad \phi_2(\xi) = \sum_{n=0}^{\infty} b_n(\xi^n + \xi^{-n}) \tag{15}$$

In the following equations, since the constants b_0 and d_0 make no contribution to the calculation of stresses, they will be taken to be zero. The problem is then reduced to the determination of the complex coefficients d_n and b_n ($n = 1, 2$). The interface condition (9) can be rewritten as

$$\Phi_1(\xi) = \delta\Phi_2(\xi) + (\delta - 1)\overline{\Phi_2(\xi)} = \beta\left[\xi\Phi_2'(\xi) + \bar{\xi}\overline{\Phi_2'(\xi)}\right] + \omega m(\xi) + \overline{\omega m(\xi)}, \quad |\xi| = R^* \tag{16}$$

Using (13) and (15), the left-hand side of Eq. (16) becomes

$$AR\xi - \delta\sum_{n=1}^{\infty} b_n \xi^n + (\delta - 1)\sum_{n=1}^{\infty} \overline{b_n}\,\bar{\xi}^{-n} + \sum_{n=1}^{\infty} d_n \xi^{-n} - \delta\sum_{n=1}^{\infty} b_n \xi^{-n} + (\delta - 1)\sum_{n=1}^{\infty} \overline{b_n}\,\bar{\xi}^{n}$$

Since the above expression is real, we obtain (setting $\xi = R^* e^{i\theta}$),

$$d_1 = \bar{A}R(R^*)^2 + (2\delta - 1)\left[b_1 - \bar{b}_1(R^*)^2\right] \quad \text{when } n = 1 \tag{17}$$

$$d_n = (2\delta - 1)\left[b_n - \bar{b}_n(R^*)^{2n}\right] \quad \text{when } n \neq 1 \tag{18}$$

Using the expressions (17) and (18) to eliminate d_n ($n = 1, 2\ldots$), the left-hand side of Eq. (16) becomes

$$\Phi_1(\xi) - \delta\Phi_2(\xi) + (\delta - 1)\overline{\Phi_2(\xi)} = RR^*\left(A\,\mathrm{e}^{i\theta} + \bar{A}\,\mathrm{e}^{-i\theta}\right) - \delta\sum_{n=1}^{\infty}\left[b_n\,\mathrm{e}^{in\theta} + \bar{b}_n\,\mathrm{e}^{-in\theta}\right](R^*)^n + (\delta - 1)\sum_{n=1}^{\infty}(R^*)^{-n}\left[\bar{b}_n\,\mathrm{e}^{in\theta} + b_n\,\mathrm{e}^{-in\theta}\right], \quad |\xi| = R^*. \tag{19}$$

Noting Eqs. (6), (12) and (16) and setting $\xi = R^*\,\mathrm{e}^{i\theta}$, the interface condition (16) is further reduced to:

$$\sqrt{1+b^*\sin^2\theta}\left\{RR^*\left[\left(A-\omega-\frac{\bar{\omega}}{R^{*2}}\right)\mathrm{e}^{i\theta}+\left(\bar{A}-\bar{\omega}-\frac{\omega}{R^{*2}}\right)\mathrm{e}^{-i\theta}\right]-\sum_{n=1}^{\infty}\delta\left[b_n\,\mathrm{e}^{in\theta}+\bar{b}_n\,\mathrm{e}^{-in\theta}\right](R^*)^n\right.$$
$$\left.+\sum_{n=1}^{\infty}(\delta-1)(R^*)^{-n}\left[\bar{b}_n\,\mathrm{e}^{in\theta}+b_n\,\mathrm{e}^{-in\theta}\right]\right\}=\sum_{n=1}^{\infty}\frac{\alpha n}{b}\left[(R^*)^n\left(b_n\,\mathrm{e}^{in\theta}\right.\right.$$
$$\left.\left.+\bar{b}_n\,\mathrm{e}^{-in\theta}\right)-(R^*)^{-n}\left(b_n\,\mathrm{e}^{-in\theta}+\bar{b}_n\,\mathrm{e}^{in\theta}\right)\right] \tag{20}$$

Substituting the expression (see Appendix A)

$$\sqrt{1+b^*\sin^2\theta}=\sum_{k=-\infty}^{\infty}I_{2k}\,\mathrm{e}^{i2k\theta}\approx\sum_{k=0}^{M-1}I_{2k}\left(\mathrm{e}^{i2k\theta}+\mathrm{e}^{-i2k\theta}\right)$$
$$+I_{2M}\frac{\mathrm{e}^{i2M\theta}+\mathrm{e}^{-i2M\theta}-\eta\left(\mathrm{e}^{i2(M-1)\theta}+\mathrm{e}^{i2(1-M)\theta}\right)}{1+\frac{1}{R^{*4}}-\frac{\mathrm{e}^{i2\theta}+\mathrm{e}^{-i2\theta}}{R^{*2}}} \tag{21}$$

into Eq. (20) (here M is a sufficiently large integer) and letting $T=A-\omega-\frac{\bar{\omega}}{R^{*2}}$, we obtain

$$RR^*\left\{\sum_{k=0}^{M-1}I_{2k}\left(\mathrm{e}^{i2k\theta}+\mathrm{e}^{-i2k\theta}\right)\left[1+\frac{1}{R^{*4}}-\frac{\mathrm{e}^{i2\theta}+\mathrm{e}^{-i2\theta}}{R^{*2}}\right]+I_{2M}\left[\mathrm{e}^{i2M\theta}+\mathrm{e}^{-i2M\theta}-\eta\left(\mathrm{e}^{i2(M-1)\theta}\right.\right.\right.$$
$$\left.\left.\left.+\mathrm{e}^{i2(1-M)\theta}\right)\right]\right\}\times\left(T\,\mathrm{e}^{i\theta}+\bar{T}\,\mathrm{e}^{-i\theta}\right)=\delta\left\{\sum_{k=0}^{M-1}I_{2k}\left(\mathrm{e}^{i2k\theta}\right.\right.$$
$$\left.+\mathrm{e}^{-i2k\theta}\right)\left[1+\frac{1}{R^{*4}}-\frac{\mathrm{e}^{i2\theta}+\mathrm{e}^{-i2\theta}}{R^{*2}}\right]+I_{2M}\left[\mathrm{e}^{i2M\theta}+\mathrm{e}^{-i2M\theta}-\eta\left(\mathrm{e}^{i2(M-1)\theta}\right.\right.$$
$$\left.\left.\left.+\mathrm{e}^{i2(1-M)\theta}\right)\right]\right\}\times\sum_{n=1}^{\infty}\left[b_n\,\mathrm{e}^{in\theta}+\bar{b}_n\,\mathrm{e}^{-in\theta}\right](R^*)^n+(1-\delta)\times\left\{\sum_{k=0}^{M-1}I_{2k}\left(\mathrm{e}^{i2k\theta}\right.\right.$$
$$\left.+\mathrm{e}^{-i2k\theta}\right)\left[1+\frac{1}{R^{*4}}-\frac{\mathrm{e}^{i2\theta}+\mathrm{e}^{-i2\theta}}{R^{*2}}\right]+I_{2M}\left[\mathrm{e}^{i2M\theta}+\mathrm{e}^{-i2M\theta}-\eta\left(\mathrm{e}^{i2(M-1)\theta}\right.\right.$$
$$\left.\left.\left.+\mathrm{e}^{i2(1-M)\theta}\right)\right]\right\}\times\sum_{n=1}^{\infty}\left[\bar{b}_n\,\mathrm{e}^{in\theta}+b_n\,\mathrm{e}^{-in\theta}\right](R^*)^{-n}+\frac{\alpha}{b}\left[1+\frac{1}{R^{*4}}-\frac{\mathrm{e}^{i2\theta}+\mathrm{e}^{-i2\theta}}{R^{*2}}\right]\times\sum_{n=1}^{\infty}n\left[b_n\,\mathrm{e}^{in\theta}\right.$$
$$\left.+\bar{b}_n\,\mathrm{e}^{-in\theta}\right](R^*)^n-\frac{\alpha}{b}\left[1+\frac{1}{R^{*4}}-\frac{\mathrm{e}^{i2\theta}+\mathrm{e}^{-i2\theta}}{R^{*2}}\right]\sum_{n=1}^{\infty}n\left[\bar{b}_n\,\mathrm{e}^{in\theta}+b_n\,\mathrm{e}^{-in\theta}\right](R^*)^{-n} \tag{22}$$

Furthermore, noting that $I_{2k}=I_{-2k}$, and equating coefficients of $\mathrm{e}^{in\theta}$ in the interface condition (22), we finally obtain

$$\sum_{j=0}^{m-1/2}\left(\sum_{k=0}^{M}D_{nkj}I_{2k}+G_{nj}\right)b_{2j+1}+\sum_{j=0}^{m-1/2}\left(\sum_{k=0}^{M}E_{nkj}I_{2k}+P_{nj}\right)\bar{b}_{2j+1}=\sum_{k=0}^{M}F_{nk}I_{2k} \tag{23}$$

Here, $n = 1,3,5\ldots m$, where m is odd and always less than M; D_{nkj}, E_{nkj} are real constants; G_{nj}, P_{nj} are real constants related to the imperfect interface parameter h and F_{nk} are complex constants. For example, by comparing Eqs. (22) and (23), when $M = 5$, $n = 3$ ($m = 5$), we obtain

$$D_{300} = -\frac{\delta}{R^*};\ D_{310} = \delta R^* + \frac{2\delta - 1}{R^{*3}};\ D_{320} = \frac{(1-2\delta)}{R^*} + \frac{1-\delta}{R^{*5}};\ D_{330} = -\frac{1-\delta}{R^{*3}};\ D_{340} = D_{350} = 0;\ G_{30} = -\frac{\alpha}{bR^*}$$

$$E_{300} = -\frac{1-\delta}{R^{*3}};\ E_{310} = \frac{1-\delta}{R^{*5}} - \frac{2\delta - 1}{R^*};\ E_{320} = \delta R^* + \frac{2\delta - 1}{R^{*3}};\ E_{330} = -\frac{\delta}{R^*};\ E_{340} = E_{350} = 0;\ P_{30} = \frac{\alpha}{bR^{*3}}$$

$$D_{301} = \delta\left(R^{*3} + \frac{1}{R^*}\right);\ D_{311} = -2\delta R^* - \frac{1-\delta}{R^{*5}};\ D_{321} = -\frac{1-\delta}{R^{*5}};\ D_{331} = (1-\delta)\left(\frac{1}{R^{*3}} + \frac{1}{R^{*7}}\right);\ D_{341} = D_{351} = 0;$$

$$G_{31} = \frac{3\alpha}{b}\left(R^{*3} + \frac{1}{R^*}\right)$$

$$E_{301} = (1-\delta)\left(\frac{1}{R^{*3}} + \frac{1}{R^{*7}} - \frac{1}{R^{*5}}\right);\ E_{311} = \frac{1-\delta}{R^{*5}};\ E_{321} = \delta R^*;\ E_{331} = \delta\left(R^{*3} + \frac{1}{R^*}\right);\ E_{341} = -\delta R^*;\ E_{351} = 0;$$

$$P_{31} = -\frac{3\alpha}{b}\left(\frac{1}{R^{*3}} + \frac{1}{R^{*7}}\right)$$

$$D_{302} = -\delta R^{*3};\ D_{312} = \delta\left(R^{*5} + R^*\right);\ D_{322} = -\delta R^{*3};\ D_{332} = -\frac{1-\delta}{R^{*5}};\ D_{342} = (1-\delta)\left(\frac{1}{R^{*5}} + \frac{1}{R^{*9}}\right);$$

$$D_{352} = -\frac{1-\delta}{R^{*5}}\eta;\ G_{32} = -\frac{5\alpha}{b}R^{*5}$$

$$E_{302} = -(1-\delta)\frac{1}{R^{*7}};\ E_{312} = (1-\delta)\left(\frac{1}{R^{*5}} + \frac{1}{R^{*9}}\right);\ E_{322} = -(1-\delta)\frac{1}{R^{*7}};\ E_{332} = \delta R^{*3};\ E_{342} = \delta\left(R^{*5} + R^*\right);$$

$$E_{352} = -\delta R^{*5}\eta;\ P_{32} = \frac{5\alpha}{b}\frac{1}{R^{*7}}$$

$$F_{30}=0;\ F_{31}=T\left(1+\frac{1}{R^{*4}}\right)-\frac{\bar{T}}{R^{*2}};\ F_{32}=\bar{T}\left(1+\frac{1}{R^{*4}}\right)-\frac{T}{R^{*2}};\ F_{33}=-\frac{\bar{T}}{R^{*2}};\ F_{34}=F_{35}=0$$

5. Numerical examples and discussion

We compute (numerically) the complex coefficients of the Laurent series in Eq. (15) for a wide range of imperfect interface parameters and aspect ratios a/b.

5.1. The case of remote mechanical loading

We consider first the case of remote loading in the absence of any eigenstrain inside the inclusion. That is, when $T=A$, $\bar{T}=\bar{A}$.

Let $b=1$ and consider the case of an epoxy matrix surrounding a glass inclusion. The material properties of the matrix and the inclusion are described by:

$$E_1=2.76\ \text{Gpa},\quad \nu_1=0.35,\quad \mu_1=1.02\ \text{Gpa}$$

$$E_2=72.4\ \text{Gpa},\quad \nu_2=0.2,\quad \mu_2=30.17\ \text{Gpa},$$

where, E is Young's modulus and ν is Poisson's ratio.

It is well known that, in the case of a perfectly bonded interface, the stress and strain fields inside an elliptic inclusion are uniform (see, for example, Ru and Schiavone, 1996). In fact, when $h=\infty$ ($\alpha=0$, perfect bonding) and $G_{nj}=P_{nj}=0$ in (23), we obtain

$$\delta R^{*}b_1+\frac{1-\delta}{R^{*}}\bar{b}_1=ARR^{*},\quad b_1=\frac{R}{\delta}\frac{A-\delta^{*}\bar{A}}{1-\delta^{*2}},\quad b_3=b_5=\cdots=0\quad \text{where } \delta^{*}=\frac{1-\delta}{\delta R^{*2}}$$

Consequently,

$$\Phi_2=b_0+\frac{R}{\delta}\frac{A-\delta^{*}\bar{A}}{1-\delta^{*2}}\frac{z}{R},$$

which coincides with the result obtained in Ru and Schiavone (1996) for an elliptic inclusion with perfectly bonded interface.

In practice, the imperfect interface parameter h is rendered dimensionless by division μ_1/b, where μ_1 is the shear modulus of the matrix and b is the minor axis of the ellipse.

In the case of the homogeneously imperfect interface, numerical computation of the corresponding series demonstrates that the non-uniformity of the stress field inside the inclusion depends significantly on the aspect ratio of the ellipse and the imperfect interface parameter.

In what follows, we present results for three different ranges of the aspect ratio a/b. In each case, the number of coefficients in the corresponding series is chosen so that, the error in the numerical calculations is maintained below 1%. This is achieved simply by calculating an increasing sequence of partial sums from each of the (uniformly convergent) infinite series representations, and noting the minimum number of coefficients required to ensure that the difference between any two subsequent partial sums is less than 1%.

Case 1. When $1<a/b\leq 3$, only the coefficients b_1 and b_3 are necessary to achieve the desired accuracy.

In this case, we find that

$$\Phi_2 \approx b_0 + (b_1 - 3b_3)\left(\frac{z}{R}\right) + b_3\left(\frac{z}{R}\right)^3 \tag{24}$$

We obtain values of b_1 and b_3 by selecting $m = 3$ and $M = 7$ in Eq. (23). It should be noted that the result for $a/b = 1$ cannot be obtained directly from the numerical analysis but is available analytically. The relationship between average stress and the imperfect parameter h, in this case, is given in Fig. 2. The average stress inside the inclusion is defined as

$$\bar{\sigma}_{ij} = \frac{\int_A \sigma_{ij} \mathrm{d}A}{A} \tag{25}$$

where A is the area of the ellipse.

In Figs. 3 and 4, the stress distribution along the interface and the regions of the ellipse described by the lines $x = 0$ and $y = 0$ is plotted for the value $a/b = 3$ and different values of the parameter h. It is clear that the non-uniformity of the stresses inside the inclusion is very strong. In fact, when $h = 5E + 5$, the local stresses reach maximum values.

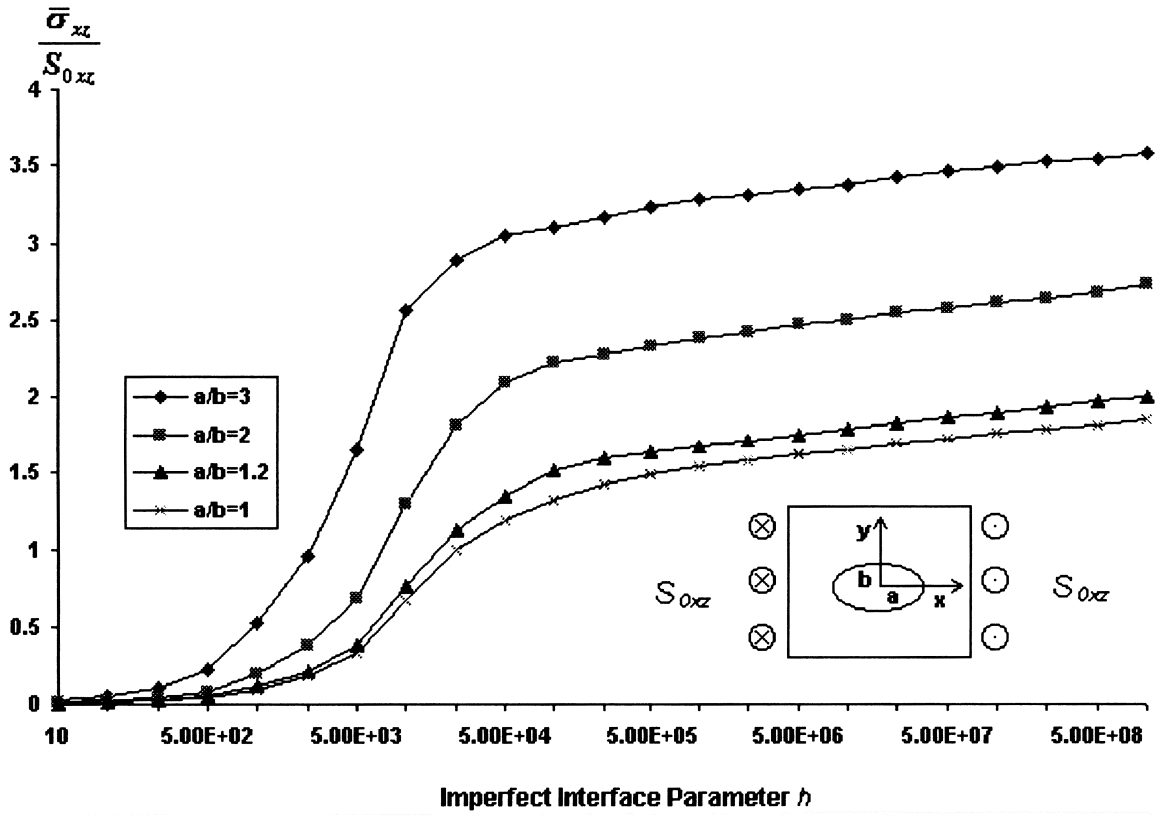

Fig. 2. Effect of the imperfect interface parameter h on the average stress ($\frac{\bar{\sigma}_{xz}}{S_{0xz}}$) inside inclusion when the remote stress is S_{0xz}.

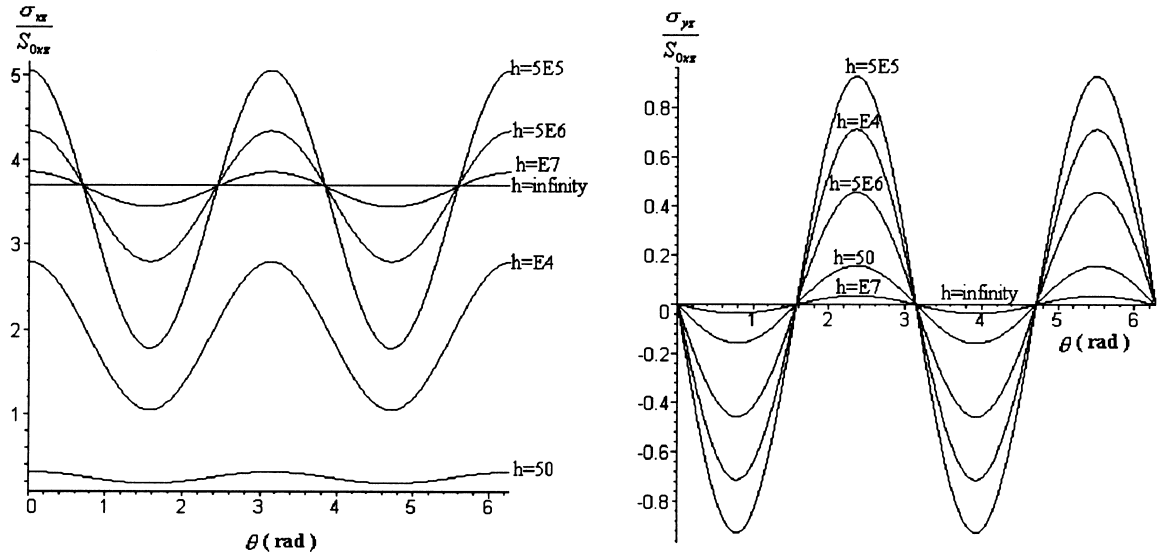

Fig. 3. Non-uniformity of stress along the interface when the remote stress is S_{0xz} with $a/b = 3$.

Case 2. When $3 < a/b \leq 6$, it is sufficient to consider only the coefficients b_1, b_3 and b_5 to obtain the required accuracy. In this case, we obtain

$$\Phi_2 \approx b_0 + (b_1 - 3b_3 + 5b_5)\left(\frac{z}{R}\right) + (b_3 - 5b_5)\left(\frac{z}{R}\right)^3 + b_5\left(\frac{z}{R}\right)^5 \tag{26}$$

We may obtain values of b_1, b_3 and b_5 by selecting $m = 5$ and $M = 9$ in Eq. (23). The corresponding stress distributions are presented in Figs. 5–7.

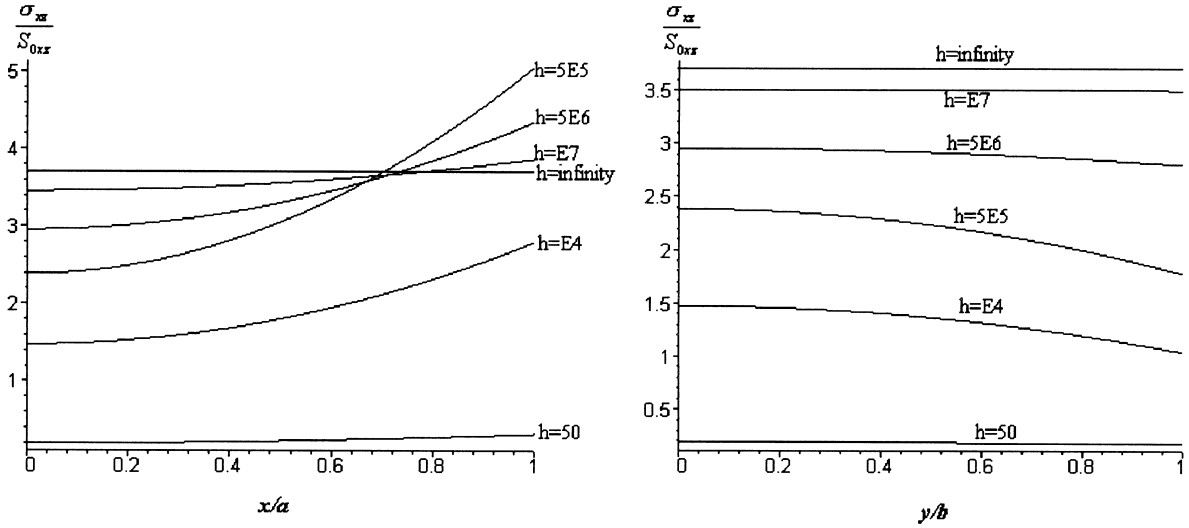

Fig. 4. The stress distribution along the x and y axes for remote stress S_{0xz} with $a/b = 3$.

Case 3. When $6 < a/b \leq 9$, only b_1, b_3, b_5 and b_7 are required to obtain the desired accuracy. In this case, we obtain

$$\Phi_2 \approx b_0 + (b_1 - 3b_3 + 5b_5 + 28b_7)\frac{z}{R} + (b_3 - 5b_5 + 14b_7)\left(\frac{z}{R}\right)^3 + (b_5 - 7b_7)\left(\frac{z}{R}\right)^5 + b_7\left(\frac{z}{R}\right)^7 \tag{27}$$

We may obtain values of b_1, b_3, b_5 and b_7 by selecting $m = 7$, $M = 11$ in Eq. (23). The corresponding stress distributions are presented in Figs. 8–10.

It is noted that for values of the aspect ratio $a/b \geq 10$, the procedure is similar although a much larger number of coefficients is required to evaluate the corresponding series to the desired accuracy.

The above results indicate that the average stress alone is insufficient to describe the debonding and failure of the interface. It is the local stress (maximum) that decides where the debonding and failure will occur. For example, from the stress distribution along the interface in Fig. 9, the maximum local stresses occur at $\theta = 0, \pi$. These stresses are much greater than those in the case of perfect bonding although the average stresses (see Fig. 8) are smaller. From Figs. 2, 5 and 8, it is clear that the effect of the imperfect interface parameter h on the average stress inside the inclusion increases with the aspect ratio of the ellipse.

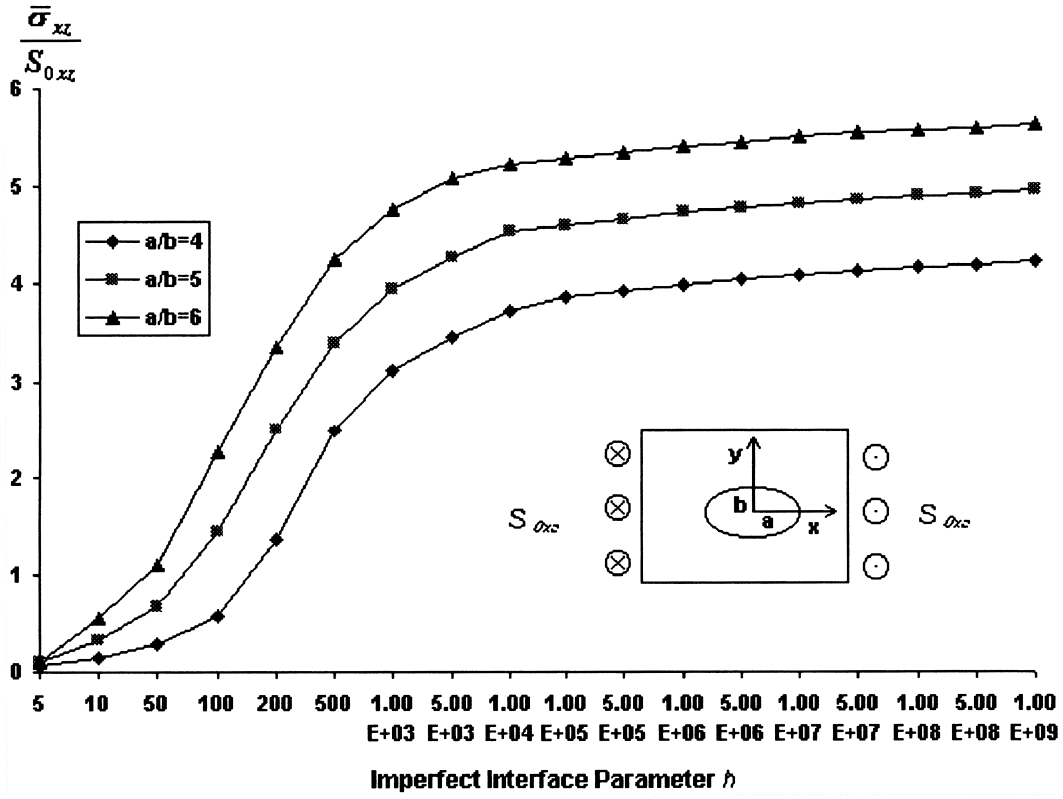

Fig. 5. Effect of the imperfect interface parameter h on the average stress ($\frac{\bar{\sigma}_{xz}}{S_{0xz}}$) inside inclusion, when the remote stress is S_{0xz}.

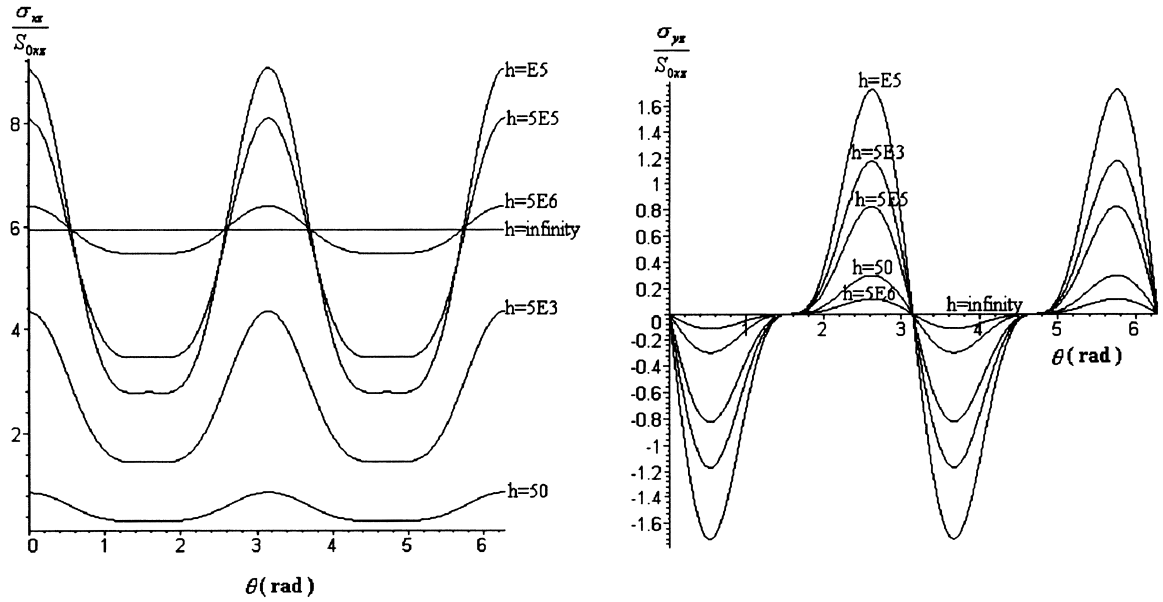

Fig. 6. Non-uniformity of stress along the interface when the remote stress is S_{0xz} with $a/b = 6$.

It should be emphasized that the imperfect interface condition (1) arises from the assumption of a thin flexible coating of thickness $t \ll b$ with shear modulus $\mu_c \ll \min\{\mu_1, \mu_2\}$ between the inclusion and the matrix (Hashin, 1991b). This defines the physical meaning of the parameter h. In practice, the interface model may be represented by an adhesive layer. For the present case, h is in the range $1E+0$ to $1E+6$, which demonstrates that the stress field is closely related to this physical meaning of h. In addition, the local stresses along the (imperfect) interface itself reach maximum values when the interface parameter h reaches a particular value (h^*). For the example under consideration, the relationship between the parameter h^* and the aspect ratio a/b is represented in Fig. 11.

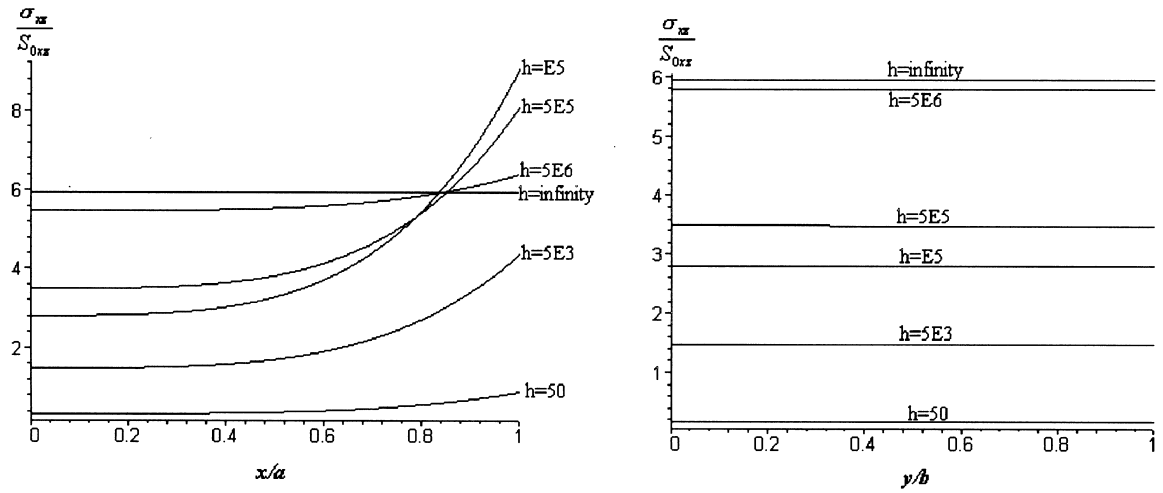

Fig. 7. stress distribution along the x and y axes for remote stress S_{0xz} with $a/b = 6$.

Since values of h^* correspond to local maximum stress and are related to the mechanical properties and thickness of the adhesive layer between the inclusion and the matrix, the parameter h^* may be used as a control parameter when designing composites involving elastic inclusions. For example, for the remote loading S_{0xz} and aspect ratio $a/b = 1$ (circular inclusion), the peak stress corresponds to the value $h^* = \infty$ (perfect bonding). However, when $a/b = 3$, the peak stress corresponds to $h^* = 5E + 5$. Since h^* is rendered dimensionless by division μ_1/b, for a specific aspect ratio, we could avoid the peak stress by adjusting μ_1 (the shear moduli of the matrix), and the thickness of the interphase layer (related to b).

In order to better understand the relationship between the imperfect interface parameter h and the failure of the interface, Fig. 12 plots the peak stresses as a function of the imperfect interface parameter. These peak stresses are calculated at the values $\theta = 0$ or π and correspond to the effective stresses which are defined by the relation $\sigma_{\text{effective}} = \sqrt{\sigma_{xz}^2 + \sigma_{yz}^2}$. In Figs. 3, 6 and 9, we note that the values of $\frac{\sigma_{yz}}{S_{0xz}}$ are much smaller than the corresponding values of $\frac{\sigma_{xz}}{S_{0xz}}$, when the remote stress is S_{0xz}. Thus, the effective stresses are mainly determined by $\frac{\sigma_{xz}}{S_{0xz}}$. Furthermore, at the values $\theta = 0$ or π, the effective stresses is equal to the values of $\frac{\sigma_{xz}}{S_{0xz}}$, because the values of $\frac{\sigma_{yz}}{S_{0xz}}$ are zero. The maximum peak stresses in Fig. 12 correspond to values of the parameter h^*. For the circular inclusion, we know that the maximum peak stress appears at $h = \infty$ (see Ru and Schiavone, 1997). However, for the elliptic inclusion, the maximum peak stresses are related to the imperfect interface parameter and the aspect ratio. To explain this, we note that for the present interphase layer model (Hashin, 1991b), in order to keep the thickness of the

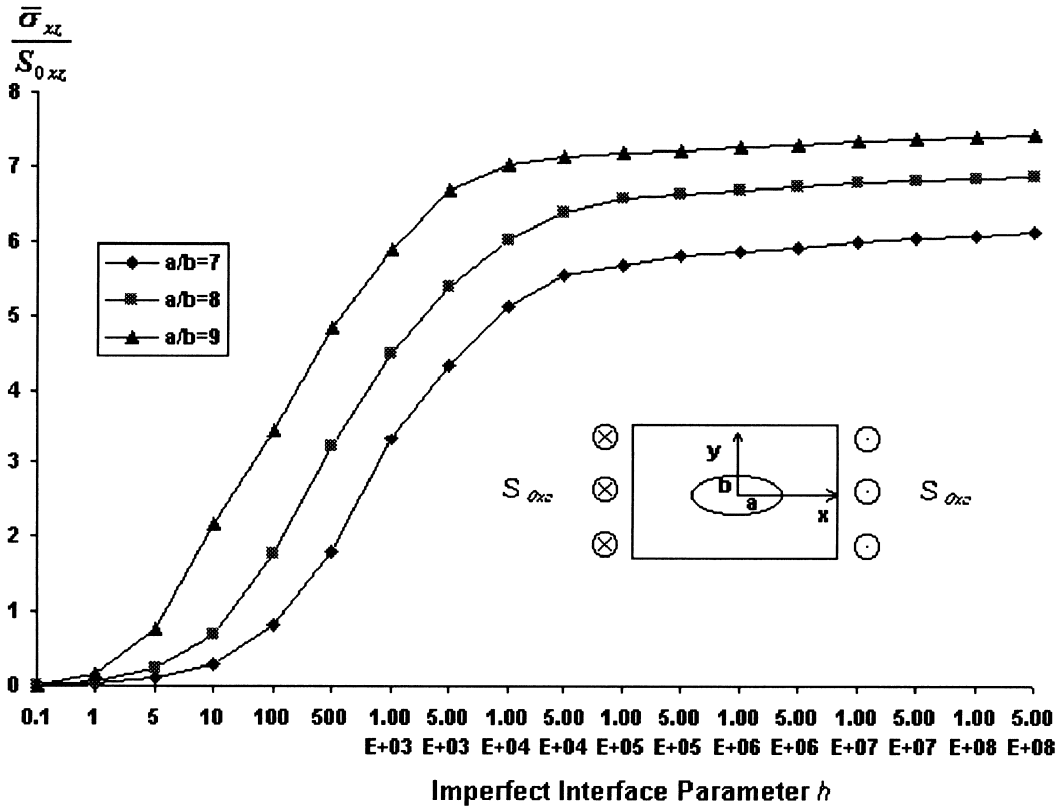

Fig. 8. Effect of the imperfect interface parameter h on the average stress ($\frac{\bar{\sigma}_{xz}}{S_{0xz}}$) inside the inclusion when the remote stress is S_{0xz}.

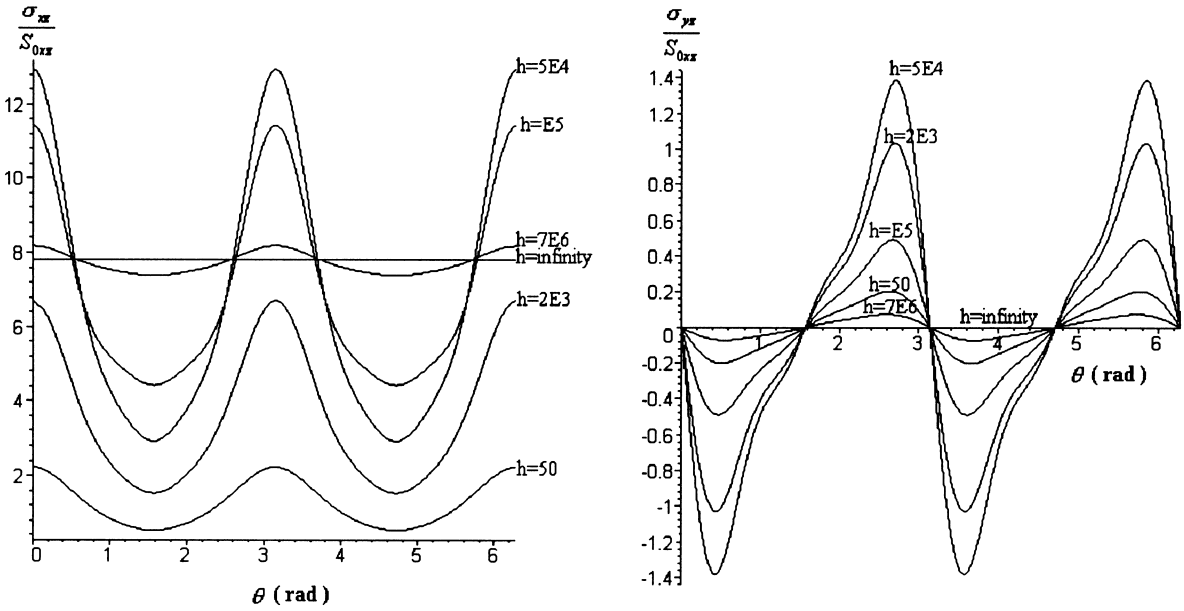

Fig. 9. Non-uniformity of stress along the interface when the remote stress is S_{0xz} with $a/b = 9$.

adhesive layer between the elliptic inclusion and the matrix uniform, unlike the innermost edge, the outer edge of the interphase layer cannot be elliptical. This is why, in the case of a homogeneously imperfect interface, values of h^* correspond to different local maximum stresses for different values of the aspect ratio a/b (for the circular inclusion with homogeneously imperfect interface, the outer edge of

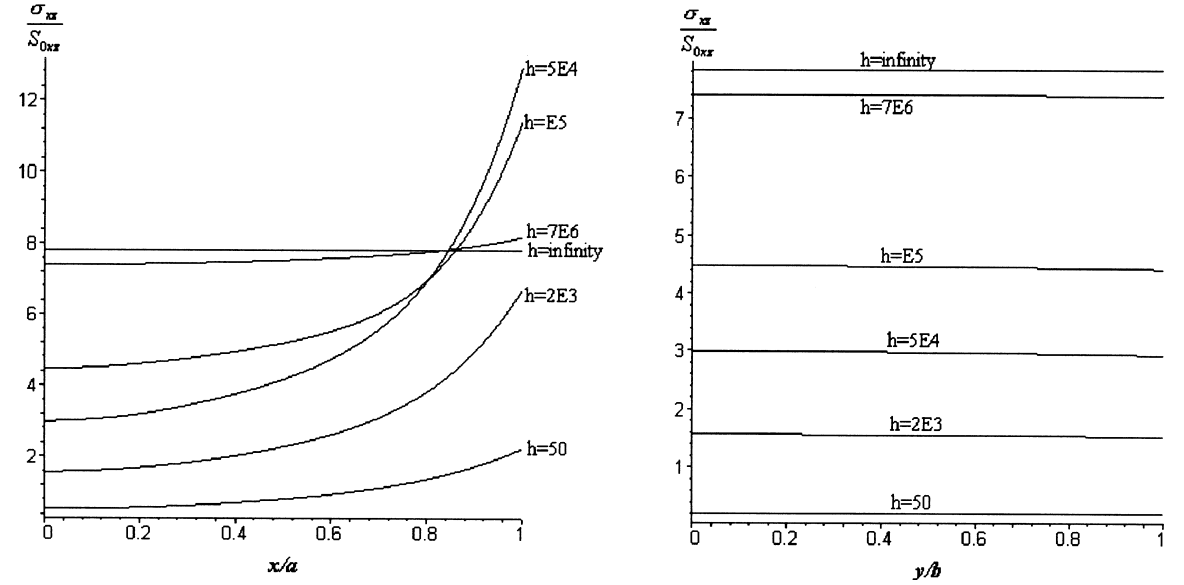

Fig. 10. The stress distributions along the x and y axes for the remote stress S_{0xz} with $a/b = 9$.

the interphase layer is circular). This makes the stress distributions along the interface extremely complicated in the case of an elliptic inclusion.

5.2. Eigenstrain problem

By a suitable choice of eigenstrain in S_2, the problem considered in Section 5.1 (remote loading with no eigenstrain in S_2) can be shown to be equivalent (in the sense that the stress field induced within S_2 is equivalent) to one in which, the remote loading is zero. In fact, if A is the remote loading parameter, we choose the eigenstrain ω such that

$$\begin{cases} \omega + \dfrac{\bar{\omega}}{R^{*2}} = -A \\ \bar{\omega} + \dfrac{\omega}{R^{*2}} = -\bar{A} \end{cases} \Longrightarrow \begin{cases} \omega = -\dfrac{R^{*2}(AR^{*2} - \bar{A})}{R^{*4} - 1} \\ \bar{\omega} = -\dfrac{R^{*2}(\bar{A}R^{*2} - A)}{R^{*4} - 1} \end{cases} \tag{28}$$

It is worth noting that for the above condition, the stress distribution in the eigenstrain problem is equivalent (to that with remote loading and no eigenstrain in S_2) only within the inclusion, and not in the matrix. For example, the stress distribution in the matrix along the x-axis, in the case when $a/b = 3$, is presented in Fig. 13. In the case of remote mechanical loading, all stresses in the matrix tend to $\frac{\sigma_{xz}}{S_{0xz}} =$

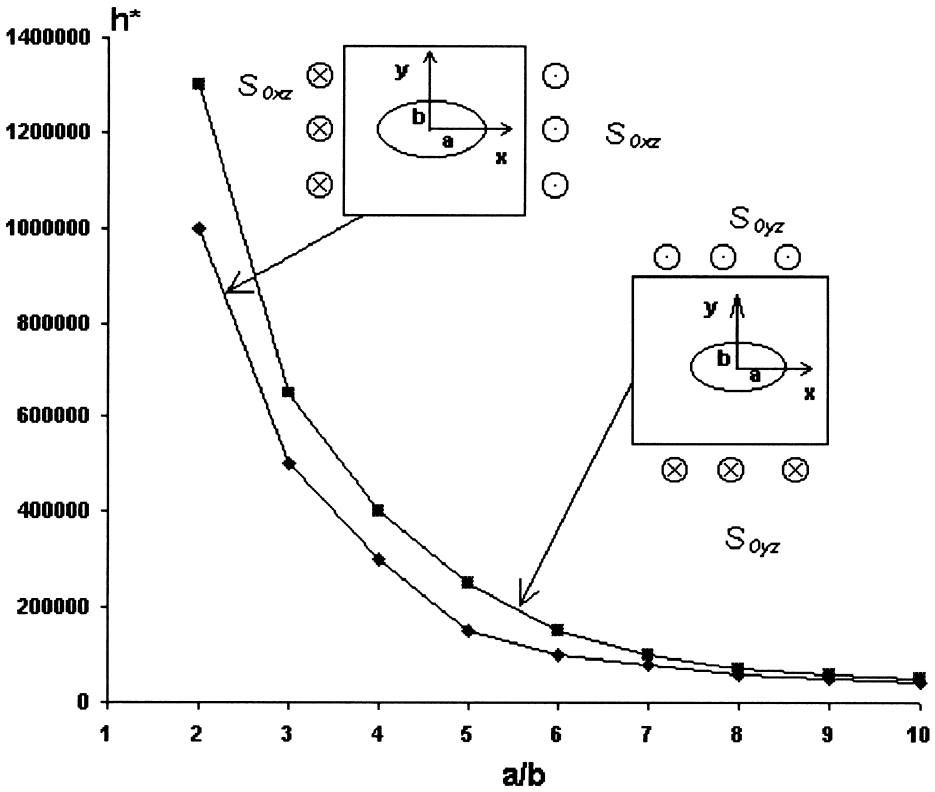

Fig. 11. The relationship between h^* and a/b.

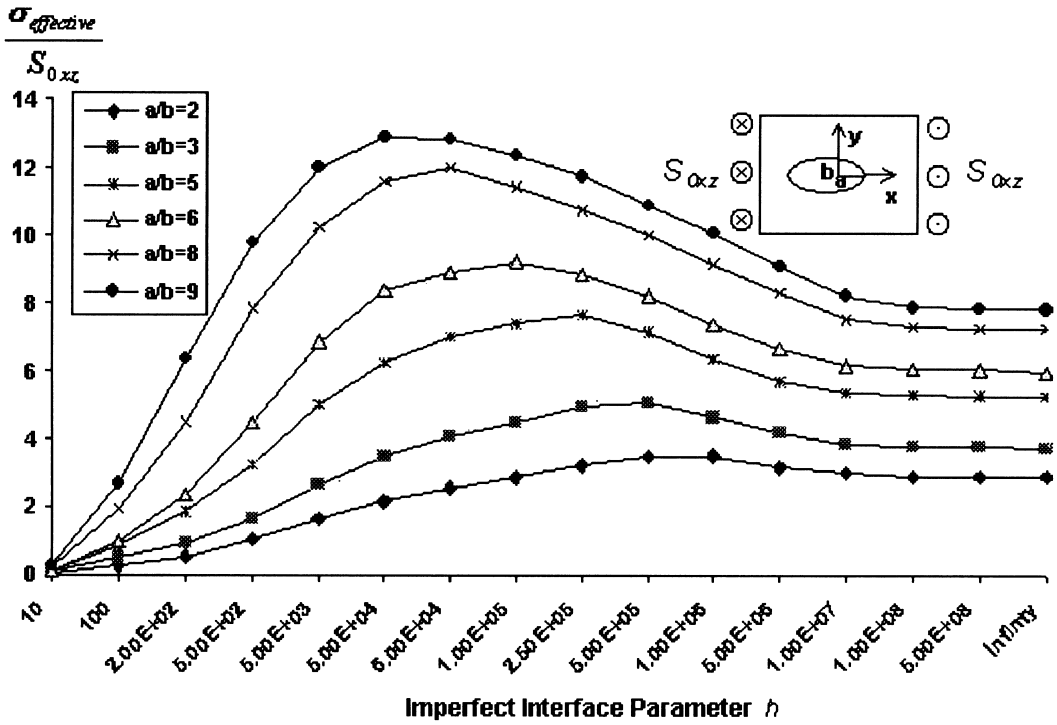

Fig. 12. The effective peak stress along the interface varies as a function of the imperfect interface parameter h when the remote stress is S_{0xz}.

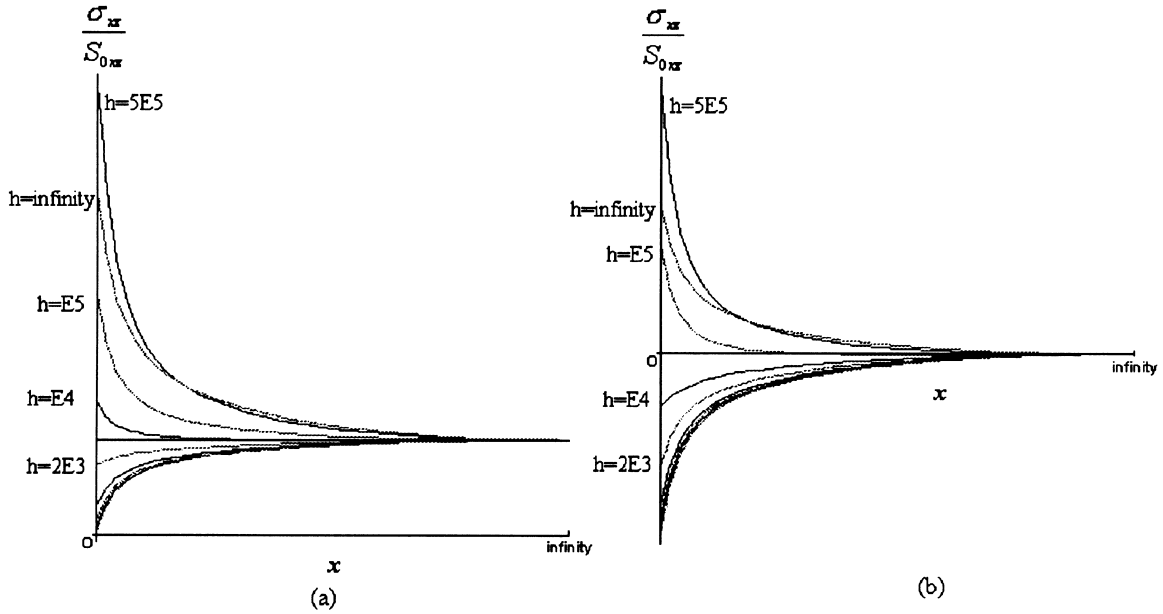

Fig. 13. The stress distribution with $a/b = 3$ for the matrix along x axis with different h when: (a) remote mechanical loading S_{0xz}; (b) eigenstrain loading.

1 when x tends to infinity, as expected. On the other hand, for the eigenstrain loading, all stresses tend to $\frac{\sigma_{xz}}{S_{0xz}} = 0$ in the similar situation.

6. Conclusions

This paper presents a semi-analytic solution of the problem of an elliptic inclusion with homogeneously imperfect interface in anti-plane shear. The results show that the interface imperfection has a significant effect on stress fields in and near the inclusion (along the interface). The non-uniformity of stress is closely related to the interface parameter describing the imperfection and the aspect ratio of the ellipse. It has also been indicated that the definition of the imperfect interface and the physical explanation of the interface parameters used in Hashin (1991b) are indeed suitable for describing the nature of the interface.

Our calculations show that using only average stress is insufficient to describe the debonding and failure of the material interface, since both are controlled by interfacial stresses which are themselves closely related to the imperfect interface condition. Furthermore, it has been shown that the effect of the imperfect interface parameter h on the average stress inside the inclusion increases with the aspect ratio of the ellipse. In particular, our results indicate that it is possible to predict and control the debonding and failure of the interface by identifying a distinct value (h^*) of the interface parameter which depends on the aspect ratio of the ellipse and the properties and thickness of the adhesive layer between the elliptical inclusion and the matrix. This is a direct consequence of the fact that values of h^* correspond to maximum peak stress along the interface. Furthermore, we have shown that, for a specific aspect ratio, it is possible to avoid or minimize peak interfacial stress by adjusting μ_1 (the shear modulus of the matrix) and the thickness of the interphase layer.

Appendix A. Infinite series representation for the expression $\sqrt{1 + b^*\sin^2\theta}$

In order to solve the Eq. (20) using infinite series, it is necessary to find a series representation for the expression $\sqrt{1 + b^*\sin^2\theta}$. To this end, note that for any integer k,

$$\int_0^{2\pi} \sqrt{1 + b^*\sin^2\theta}\sin k\theta \mathrm{d}\theta = 0,$$

$$\int_0^{2\pi} \sqrt{1 + b^*\sin^2\theta}\cos(2k+1)\theta \mathrm{d}\theta = 0. \tag{A1}$$

Thus,

$$\int_0^{2\pi} \sqrt{1 + b^*\sin^2\theta}\cos\big[2(k+1)\big]\theta \mathrm{d}\theta = \int_0^{2\pi} \sqrt{1 + b^*\sin^2\theta}\big[\cos(2k\theta)\cos(2\theta) - \sin(2k\theta)\sin(2\theta)\big]\mathrm{d}\theta =$$

$$\int_0^{2\pi} \sqrt{1 + b^*\sin^2\theta}\cos(2k\theta)\cos(2\theta)\mathrm{d}\theta + \frac{4k}{3b^*}\int_0^{2\pi} \sqrt{1 + b^*\sin^2\theta}\big[1 + b^*\sin^2\theta\big]\cos(2k\theta)\mathrm{d}\theta =$$

$$\frac{1}{2}\left(1-\frac{2k}{3}\right)\int_0^{2\pi}\sqrt{1+b^*\sin^2\theta}\Big[\cos\big[2(k+1)\theta\big]+\cos\big[2(k-1)\big]\Big]\mathrm{d}\theta$$
$$+\frac{2k(2+b^*)}{3b^*}\int_0^{2\pi}\sqrt{1+b^*\sin^2\theta}\cos(2k\theta)\mathrm{d}\theta \tag{A2}$$

If we define

$$I_{2k}\equiv\frac{1}{2\pi}\int_0^{2\pi}\sqrt{1+b^*\sin^2\theta}\cos(2k\theta)\mathrm{d}\theta \tag{A3}$$

we have $I_{2k}=I_{-2k}$ and

$$\left(\frac{1}{2}+\frac{k}{3}\right)I_{2(k+1)}=\left(\frac{1}{2}-\frac{k}{3}\right)I_{2(k-1)}+\frac{2k(2+b^*)}{3b^*}I_{2k} \tag{A4}$$

Next, writing

$$\sqrt{1+b^*\sin^2\theta}=\sum_{k=0}^{\infty}I_{2k}\big(\mathrm{e}^{i2k\theta}+\mathrm{e}^{-i2k\theta}\big). \tag{A5}$$

we note that, for large k, the right-hand side of Eq. (A5) approaches a geometric series. To find the ratio of this geometric series, let us assume that for large k,

$$\frac{I_{2(k+1)}}{I_{2k}}=\eta.$$

Also, for large k, Eq. (A4) can be reduced to:

$$I_{2(k+1)}=-I_{2(k-1)}+\frac{2(2+b^*)}{b^*}I_{2k}.$$

Consequently,

$$\eta^2+1-2\frac{2+b^*}{b^*}\eta=0 \tag{A6}$$

Noting the expressions for b^* and R^* in Eqs. (7) and (12), we have

$$\eta=\frac{2+b^*}{b^*}-\sqrt{\left(\frac{2+b^*}{b^*}\right)^2-1}=\frac{1}{R^{*2}}<1, \tag{A7}$$

which implies that the geometric series is convergent. We can now rewrite Eq. (A5) as:

$$\sqrt{1+b^*\sin^2\theta}=\sum_{k=0}^{M-1}I_{2k}\big(\mathrm{e}^{i2k\theta}+\mathrm{e}^{-i2k\theta}\big)+\sum_{k=0}^{\infty}I_{2(M+k)}\big[\mathrm{e}^{i2(M+k)\theta}+\mathrm{e}^{-i2(M+k)\theta}\big]$$

and consider the second term on the right-hand side as a geometric series (approximately).

Thus,

$$\sqrt{1+b^*\sin^2\theta} \cong \sum_{k=0}^{M-1} I_{2k}\left(\mathrm{e}^{i2k\theta}+\mathrm{e}^{-i2k\theta}\right)+I_{2M}\left[\frac{\mathrm{e}^{i2M\theta}}{1-\eta\,\mathrm{e}^{i2\theta}}+\frac{\mathrm{e}^{-i2M\theta}}{1-\eta\,\mathrm{e}^{-i2\theta}}\right]=$$

$$\sum_{k=0}^{M-1} I_{2k}\left(\mathrm{e}^{i2k\theta}+\mathrm{e}^{-i2k\theta}\right)+I_{2M}\frac{\mathrm{e}^{i2M\theta}+\mathrm{e}^{-i2M\theta}-\eta\left[\mathrm{e}^{i2(M-1)\theta}+\mathrm{e}^{i2(1-M)\theta}\right]}{1+\dfrac{1}{R^{*4}}-\dfrac{1}{R^{*2}}\left(\mathrm{e}^{i2\theta}+\mathrm{e}^{-i2\theta}\right)} \tag{A8}$$

The expression (A8) is sufficiently accurate for a given suitably large number M.

References

Aboudi, J., 1987. Damage in composites-modeling of imperfect bonding. Compos. Sci. Tech 28, 103–128.

Achenbach, J.D., Zhu, H., 1989. Effect of interfacial zone on mechanical behaviour and failure of fibre-reinforced composites. J. Mech. Phys. Solids 37, 381–393.

England, A.H., 1971. Complex Variable Methods in Elasticity. Wiley–Interscience, London.

Eshelby, J.D., 1957. The determination of the elastic field of an ellipsiodal inclusion and related problems. Proc. R. Soc. London A 241, 376–396.

Gao, J., 1995. A circular inclusion with imperfect interface: Eshelby's tensor and related problems. J. Appl. Mech 62, 860–866.

Hashin, Z., 1990. Thermoelastic properties of fiber composites with imperfect interface. Mech. Mater 8, 333–348.

Hashin, Z., 1991a. Thermoelastic properties of particulate composites with imperfect interface. J. Mech. Phys. Solids 39, 745–762.

Hashin, Z., 1991b. The spherical inclusion with imperfect interface. J. Appl. Mech 58, 444–449.

Hashin, Z., 1992. Extremum principles for elastic heterogeneous media with imperfect interfaces and their application to bounding of effective moduli. J. Mech. Phys. Solids 40, 767–781.

Muskhelishvili, N.I., 1963. Some Basic Problems of the Mathematical Theory of Elasticity. Noodhoff, Groningen.

Qu, J., 1993. Eshelby tensor for an elastic inclusion with slightly weakened interface. J. Appl. Mech 60, 1048–1050.

Ru, C.Q., Schiavone, P., 1996. On the elliptic inclusion in anti-plane shear. Math. Mech. Solids 1, 327–333.

Ru, C.Q., Schiavone, P., 1997. A circular inclusion with circumferentially inhomogeneous interface in antiplane shear. Proc. R. Soc. London A 453, 2551–2572.